presence of SEC was confirmed by decreasing the gain settings to exclude background noise artifact. The SEC video image was recorded as unarchived avi file into PC. The image size was 640x480 pixels (VGA) and frame rate was 30 fps.

B. Image Processing

The consecutive still frames in BMP format were made from the video file. As the preprocessing, the each frame denoised by Wiener filter [11].

In this study, to estimate blood flow vector of SEC, gradient-based optical flow estimation is used.

The Lucas-Kanade method [12] was applied as gradient-based optical flow estimation algorithm. This method is a simple yet powerful algorithm which has the advantage of less computational costs. The basic assumption in this algorithm is that the pixel intensities are constant along the motion trajectory. Hence, the displacement is calculated by computing a least squares estimate of the brightness constraint following equations for the pixels in the neighborhood.

$$uI_x + vI_y + I_t = 0 \tag{1}$$

where I_x, I_y and I_t represent the intensity gradients. (u, v) represents motion. The simplest method for computing the optical flow (u, v) is to integrate the image measurements in a neighborhood Ω of (x, y) and solve the following 2×2 linear equation using the least-squares estimation.

$$\sum_{\Omega}\begin{bmatrix} I_x^2 & I_xI_y \\ I_xI_y & I_y^2 \end{bmatrix}\begin{bmatrix} u \\ v \end{bmatrix} = -\sum_{\Omega}\begin{bmatrix} \sum I_xI_t \\ \sum I_xI_t \end{bmatrix} \tag{2}$$

After calculation of each motion vector, motion vectors ware imposed on B-mode image.

III. Result

Fig. 2 shows the blood flow vectors at mitral valve opening. It is observed that the blood in LA propagates from LA to mitral valve. Optical flow is calculated at all grid points, but the accuracy of vectors at the area where SEC is not observed or the intensity are low, e.g., part of aorta and left ventricle. Fig. 3 is the blood flow vectors of LA 60 msec (2 frames) after Fig.2. The blood flow vectors at mitral valve are very low and the propagation of blood toward into left ventricle is diminished. Optical flow represents not only SEC flow but also LA wall motion. Hence, Fig. 3 also indicates that the LA wall Besides, it is also indicate Fig. 4 shows the 2-D blood flow vectors at systole. Mitral valve is closed and the blood whiling is shown.

IV. Discussion

The LA appendage is known to be a principal site ob thrombus formation in AF. The blood flow is usually very slow and the flow pattern is complex like swirling flow in the LA appendage. In previous reports, immunoreactive von Willebrand factor (vWF) in LA was correlated to wall shear stress caused by slow blood flow [13] and was correlated with the extent of platelet adhesion/aggregation leading to stroke [14],[15]. Thus, understanding LA flow state is important to predict and prevent atrial thrombus formation leading to stroke.

Fig. 2 2-D blood flow vectors at mitral valve opening

Fig. 3 2-D blood flow vectors at 60msec after Fig. 2

2-D velocity distribution in LA was successfully obtained with proposed method. the proposed flow distribution method has two major advantages. One is that the method

can detect very slow blood flow which cannot be detected by conventional Doppler method. In this study, the resolution of flow vector is 5.3 m/sec in case that the frame rate is 30 fps and image resolution is VGA and the resolution depends on the resolution of echo image and. Hence, it is easy to improve the flow resolution by using RF signal directly. The other advantage is that the method can visualize any directions of flow vectors in image plane while conventional Doppler method can only detect the flow along the ultrasonic beam.

The Lucas-Kanade method which is applied for the proposed flow distribution has a brightness constancy assumption. Usually, this assumption is almost satisfied because SEC consists mainly of very low flow components. This means, on the other hand, the proposed method cannot detect fast flow. Besides, the flow vector is not accurate in case that the dynamically change in the texture of SEC caused by the fast blood flow in vertical direction for the image plane. Hence, the accuracy of flow vector should be evaluated and visualized in each calculation of optical flow.

One of the limitations of the proposed method is that the method cannot detect the SEC flowing in three-dimensional space. This limitation may be overcome by deducing the velocity component orthogonal to the Doppler velocity with taking the law of conservation of mass (the equation of continuity) into consideration [16].

V. Conclusion

Because the presence of SEC is one of high risk signs of thrombosis leading to stroke, it is very important to diagnose the slow blood flow in LA with SEC. We applied the conventional gradient based optical flow estimation method to the flow distribution of SEC. The results indicate that the proposed method can represent low blood flow vector that cannot be detected by conventional Doppler method.

Optical flow vectors represent not only the slow blood flow in SEC but also the motion of heart muscle including atrial wall. Therefore, the proposed method may be able to contribute a specific diagnosis of AF or a risk evaluation for heat disease and stroke.

In future study, in order to solve the problem of a brightness constancy assumption, the evaluation and visualization of accuracy of each vector should be considered. Besides, another optical flow estimation method which does not need the assumption [17] should also be appled and compared with the proposed method.

Fig. 4. 2-D flow vectors at systole

References

[1] IW. Black, AP. Hopkins, LC. Lee, and WF Walsh, "Left atrial spontaneous echo contrast: a clinical and echocardiographic analysis", J Am Coll Cardiol, 18, pp. 398-404, 1991.

[2] LM. Tsai, JH. Chen, CJ. Fang, LJ. Lin, CM. Kwan, "Clinical implications of left atrial spontaneous echo contrast in nonrheumatic atrial fibrillation," Am J Cardiol., 70(3), pp. 327-331, Aug. 1992

[3] DYG. Leung, IW. Black, GB. Cranney, AP. Hopkins, WF. Walsh, "Prognostic implications of left atrial spontaneous echo contrast in nonvalvular atrial fibrillation," J Am Coll Cardiol., 24(3), pp. 755-762, Sep. 1994.

[4] R. Castello, AC. Pearson, AJ. Labovitz, "Prevalence and clinical implications of atrial spontaneous contrast in patients undergoing transesophageal echocardiography," Am J Cardiol., 65(16), pp. 1149-1153, May 1990.

[5] SL. Archer, LR. Kvernern, K. James, M. Ezekowitz, C. Gornick, "Does warfarin reduce the prevalence of left atrial thrombus in chronic atrial fibrillation? a double blind, placebo controlled study," Circulation, 84(suppl 2), II-693, 1991

[6] D. Fatkin, RP. Kelly, MP. Feneley, "Relations between left atrial appendage blood flow velocity, spontaneous echocardiographic contrast and thromboembolic risk in vivo," J Am Coll Cardiol, 23, pp. 961-969, 1994.

[7] E. Donal, H. Yamada, C. Leclercq, and D. Herpin, "The Left Atrial Appendage, a Small, Blind-Ended Structure: A Review of Its Echocardiographic Evaluation and Its Clinical Role," Chest, 128(3), pp. 1853-1862, Sep. 2005

[8] O. Kamp, PM. Verhost, RC. Welling, CA. Visser, "Importance of left atrial appendage flow as a predictor of thromboembolic events in patients with atrial fibriation," Eur. Heart J., 20, pp. 979-985, 1999.

[9] T. Tabata, T. Oki, A. Iuchi, H. Yamada, K. Manabe, K. Fukuda, M. Abe, N. Fukuda, S. Ito, "Evaluation of left atrial appendage function by measurement of changes in flow velocity patterns after electrical cardioversion in patients with isolated atrial fibrillation," Am J Cardiol., 79(5), pp. 615-620, Mar. 1997.

[10] T. Bartel, S. Müller, HJ. Nesser, S. Möhlenkamp, C. Bruch, R. Erbel, "Usefulness of motion patterns identified by tissue Doppler echocardiography for diagnosing various cardiac masses, particularly valvular vegetations," Am J Cardiol., 84, pp. 1428-1433, 1999.

[11] Lim, Jae S., "Two-Dimensional Signal and Image Processing," Englewood Cliffs, NJ, Prentice Hall, 1990, pp. 536-540.

[12] BD. Lucas and T. Kanade, "An iterative image registration technique with an application to stereo vision," Proc. of the 7th International Joint Conference on Articial Intelligence, 1981, pp. 674-679.

[13] H. M. Tsai, I. I. Sussman, R. L. Nagel. "Shear stress enhances the proteolysis of von Willebrand factor in normal plasma.", Blood. vol. 83, 1994, pp. 2171-2179.

[14] M. Fukuchi, J. Watanabe, K. Kumagai, Y. Katori, S. Baba, K. Fukuda, T. Yagi, A. Iguchi, H. Yokoyama, M. Miura, Y. Kagaya, S. Sato, K. Tabayashi, K. Shirato. "Increased von Willebrand Factor in the endocardium as a local predisposing factor for thrombogenesis in overloaded human atrial appendage.", J. Am. Coll. Cardiol. vol. 37, 2001, pp. 1436-1442.
[15] K. Kumagai, M. Fukuchi, J. Ohta, S. Baba, K. Oda, H. Akimoto, Y. Kagaya, J. Watanabe, K. Tabayashi, K. Shirato. "Expression of the von Willebrand factor in atrial endocardium is increased in atrial fibrillation depending on the extent of structural remodeling.", Circ. J. vol. 68, 2004, pp. 321-327.
[16] S. Ohtsuki, M. Tanaka. "Doppler pressure field deduced from the Doppler velocity field in an observation plane in a fluid.", Ultrasound Med. Biol. vol. 29, 2003, pp. 1431-1438.
[17] CH. Teng, SH. Lai, YS. Chen, WH. Hsu, "Accurate optical flow computation under non-uniform brightness variations", Computer Vision and Image Understanding, 97, 2005, pp. 315-346

Proceedings of the 29th Annual International
Conference of the IEEE EMBS
Cité Internationale, Lyon, France
August 23-26, 2007.

Morphological Approach for the Functional Improvement of an Artificial Myocardial Assist Device using Shape Memory Alloy Fibres

Y. Shiraishi, T. Yambe, Y. Saijo, F. Sato, A. Tanaka, M. Yoshizawa, D. Ogawa, *Member, IEEE*
Y. Wada, S. Itoh, R. Sakata, Y. Park, M. Uematsu, M. Umezu, T. Fujimoto, N. Masumoto, H. Liu,
A. Baba, S. Konno, S. Nitta, K. Imachi, K. Tabayashi, H. Sasada and D. Homma

Abstract— **The authors have been developing a mechano-electric artificial myocardial assist system (artificial myocardium) which is capable of supporting natural contractile functions from the outside of the ventricle without blood contacting surface. In this study, a nano-tech covalent type shape memory alloy fibre (Biometal, Toki Corp, Japan) was employed and the parallel-link structured myocardial assist device was developed. And basic characteristics of the system were examined in a mechanical circulatory system as well as in animal experiments using goats. The contractile functions were evaluated with the mock circulatory system that simulated systemic circulation with a silicone left ventricular model and an aortic afterload. Hemodynamic performance was also examined in goats. Prior to the measurement, the artificial myocardial assist device was installed into the goat's thoracic cavity and attached onto the ventricular wall. As a result, the system could be installed successfully without severe complications related to the heating, and the aortic flow rate was increased by 15% and the systolic left ventricular pressure was elevated by 7% under the cardiac output condition of 3L/min in a goat. And those values were elevated by the improvement of the design which was capable of the natural morphological myocardial tissue streamlines. Therefore it was indicated that the effective assistance might be achieved by the contraction by the newly-designed artificial myocardial assist system using Biometal. Moreover it was suggested that the assistance gain might be obtained by the optimised configuration design along with the natural anatomical myocardial stream line.**

I. Introduction

In general, the artificial ventricular assist systems, such as artificial hearts, were employed for the treatment of the severe heart failure in order to increase the circulation volume. However the complications caused by the hemolysis or thrombosis on the surface of the artificial materials are still outstanding problems in the application of those de-vices to patients. Heart transplantation has also been widely performed as destination therapy for the severe heart failure. But it is limited by donor organ shortages, selection criteria, as well as the cost [1]. And recently, cell transplantation to repair or supplement impaired heart tissue has been reported as an alternative therapy for that [2]. The authors assumed that the essence of the pathophysiological development of severe heart failure was in the decrease in the cardiac contractility. Then an artificial myocardium has been developed using a covalent nano-tech shape memory alloy fibre, which is capable of assisting natural cardiac contraction from out-side of the ventricular wall as shown in Figure 1 [3]. The purpose of this study was to develop a sophisticated artificial myocardium unit, and also to have examined the hemodynamic effects of the myocardial assist system on cardiac function.

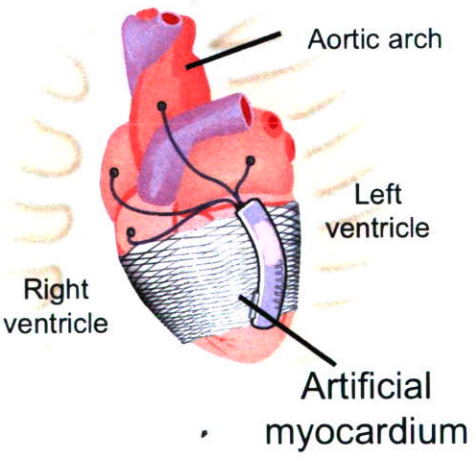

Fig. 1: Schematic illustration of an artificial myocardium attached on the ventricular wall; the synchronous contraction can be achieved according to the natural physiological demand.

This study was supported by Grant in Aid for Scientific Research of Ministry of Health, Labour and Welfare (H17-nano-009), and Ministry of Education, Culture, Sports, Science and Technology (17790938). And this study was partly supported by Grant in Aid for Scientific Research of Pharmaceuticals and Medical Devices Agency and Fujita Memorial Fund of Japan Society for the Promotion of Science..

Y. Shiraishi, T. Yambe, K. Sekine, F. Saijo, H. Liu, S. Konno, S. Nitta are with the Institute of Development, Aging and Cancer, Tohoku University, Sendai 980-8575, Japan (corresponding author to provide phone: +81 22 717 8517; fax: +81 22 717 8518; e-mail: shiraishi@idac.tohoku.ac.jp).

N. Masumoto is with the Department of Mechanical Engineering, Nippon Institute of Technology, Saitama, Japan. Y. Wada, S. Itoh, M. Uematsu, R. Sakata, Y. Park, M. Umezu are with Waseda University, Tokyo, Japan. D. Ogawa, P. Olegario, F. Sato are with the Graduate School of Engineering, Tohoku University, Sendai, Japan. M. Yoshizawa is with the Information Synergy Center, Tohoku University, Sendai, Japan. A. Tanaka is with the Faculty of Symbiotic Systems Science, Fukushima University, Fukushima, Japan. A. Baba and K. Imachi are with Tohoku University Biomedical Engineering Research Organization, Sendai, Japan. K. Tabayashi is with the Graduate School of Medicine, Tohoku University, Sendai, Japan. H. Sasada is with the Graduate School of Agriculture, Tohoku University, Sendai, Japan. T. Fujimoto is with the Shibaura Institute of Technology, Tokyo, Japan. D. Homma is with the Toki Corporation, Tokyo, Japan..

1-4244-0788-5/07/$20.00 ©2007 IEEE

The authors have been developing a totally-implantable artificial myocardial assist device [4]-[6]. The methodologies of the direct ventricular support systems were already reported as direct mechanical ventricular assistance (DVMA) by Anstadt's or other groups, as well as the right ventricular assist device which was invented and reported at IDAC, Tohoku University [7]-[9]. In this study, a design to surround the total heart has been established in order to refrain from the stress concentration by the mechanical assistance, and the hemodynamic performance of the artificial myocardial assist system were examined in a mock circulatory system as well as on animal experiments using goats. And also morphological design approach has been conducted and basic characteristics of the three types of myocardial assist device were examined so that the representation of the anatomical structure of natural myocardial tissue for more sophisticated mechanical assistance from the outside could be achieved.

II. Materials and Methods

A. Artificial Myocardium using Shape Memory Alloy Fibres

The myocardial assist system, as shown in Figure 2, consists of a covalent type shape memory alloy fibre (Biometal®). The diameter of the fibre is 100 microns, and it is contracted by the Joule heating. In general, Ti-Ni alloy is well known as a material with the shape-memory effect[10]-[12]. The fibre material is able to be covered with a silicone –tubing (diameter: 150um). The configuration of the mate-rial was basically constructed by covalent bond, so that it indicated a big strain change by 5 to 10% in length. The linearity of the recovery strain and the changes in electric resistance could be adjusted through the fabrication process, so that the strain of the fibre could be easily controlled by using the digital-servo system without potentiometers.

The layered structures are formed in the ventricular wall from the anatomical point of view as shown in Figure 3, and the effective mechanical blood flow output is achieved by the integrative anisotropic contraction from epi- to endocardium [13].

In this study, the authors developed a prototype artificial myocardium by using the shape memory alloy fibres for the simulation of such natural complicated myocardial tissue stream as shown in Figure 4. And the representation of the myocardial stream on the ventricular wall was performed by the oblique-shaped myocardial assist device.

B. Mock Circulatory Evaluation and Animal Experiments

Contractile function of the device developed was examined onto the originally-designed silicone mock left ventricle (Figure 3). Hydrodynamic evaluation was conducted against the afterload of 80 to 100mmHg without mock ventricular contraction.

Hemodyamic data were also obtained from normal adult

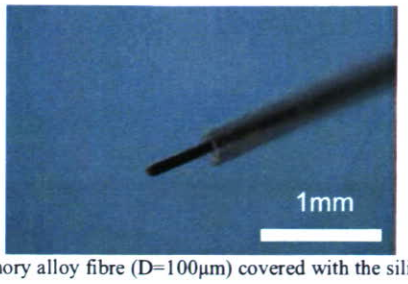

(a) Shape memory alloy fibre (D=100μm) covered with the silicone tubing

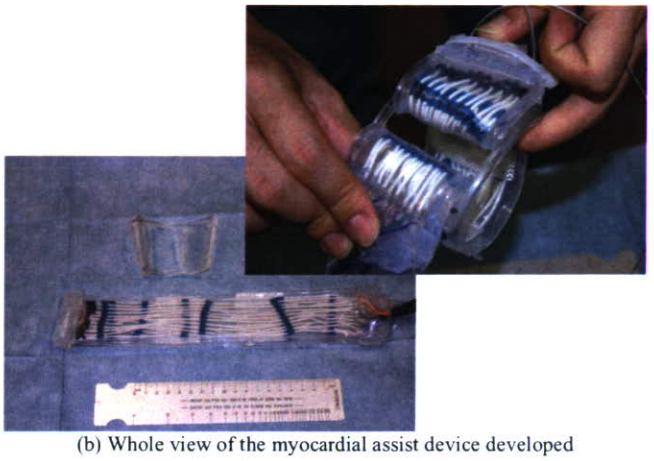

(b) Whole view of the myocardial assist device developed

Fig. 2: The mechanical component of the artificial myocardial actuator (a), and the myocardial assist device of parallel-link structure which was designed to be an active girdle for the ventricular contraction

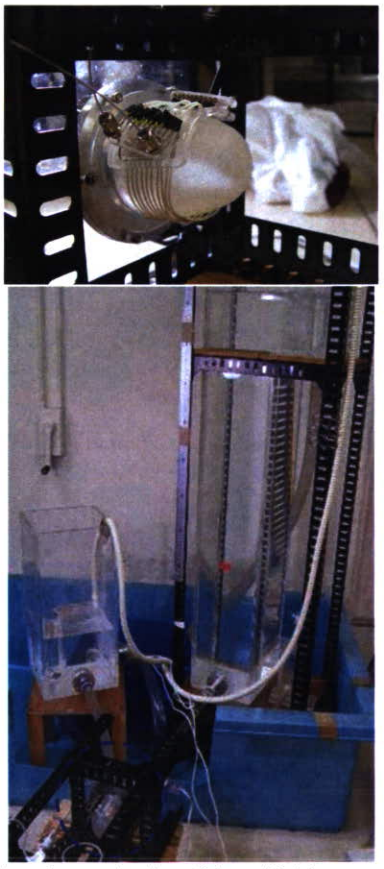

Fig. 3: Hydrodynamic examination of the artificial myocardium (top); the device was attached onto the silicone mock left ventricular model (bottom).

healthy goats, the mean weight of which was 50kg under the normal intubation and general anesthetizing process by 2.5% Fluothane. Prior to the measurement, the artificial myocardial assist device with parallel-linked shape memory alloy fibres was covered with silicone rubber, and it was attached onto the ventricular wall. Left ventricular (LV) pressure was measured by a catheter tip transducer (Millar, SVPC-664A), The sensor was inserted at the left atrial portion through the mitral valve. These hemodynamic data were recorded by a digital recording unit (TEAC, LX-10) and the sampling frequency was 0.5 - 1.5 kHz.

All the animal experiments related to this study were scrutinized and approved by the ethical committee on the animal experiment of the Department of Medicine, Tohoku University, and also the Institute of Development, Aging and Cancer, Tohoku University, 2004-2006.

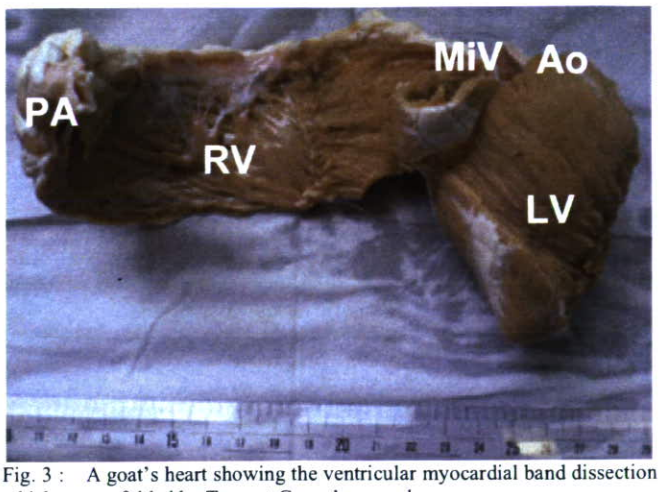

Fig. 3 : A goat's heart showing the ventricular myocardial band dissection which was unfolded by Torrent-Guasp's procedure

III. Results and Discussion

A. Effects of the displacement on the ventricular contraction and design improvement by morphological representation

Basic contraction was achieved to be 5% shortening in each fibre module. Therefore the actual displacement for ventricular assistance together with the acrylic adjustment component was estimated to be over 7%, which was similar to the displacement change obtained from the goat's ventricular surface by using our 3D measurement [14].

As shown in Figure 5, the oblique type which was able to represent the natural morphological myocardial streamline indicated the bigger output of around 5L/min against the after load of 100mmHg in the mock circulatory system.

B. Surgical procedure and hemodynamic effects on the goat's cardiovascular system

In order to achieve the effective reduction of the volume inside of the heart during the systolic phase, the changes of the ventricular wall thickness might be inevitable. Though the concept of supporting cardiac function from outside by using this artificial myocardial assist system does not involve those native thickening function of the heart, the controllable displacement of this device might be useful for more sophisticated cardiac assist.

The myocardial assist device developed was successfully installed into the goat's thoracic cavity without any complications. Hemodynamic waveforms were changed by the mechanical assistance. It was not necessary to remove any costae to install the whole actuator into the thoracic cavity, whereas one rib should be taken away during the surgical procedure of the other electrohydraulic myocardial assist system which had been developed [6]. As the actuator employed for the artificial myocardium itself was so small, the less room in the thoracic cavity might be needed. Moreover,

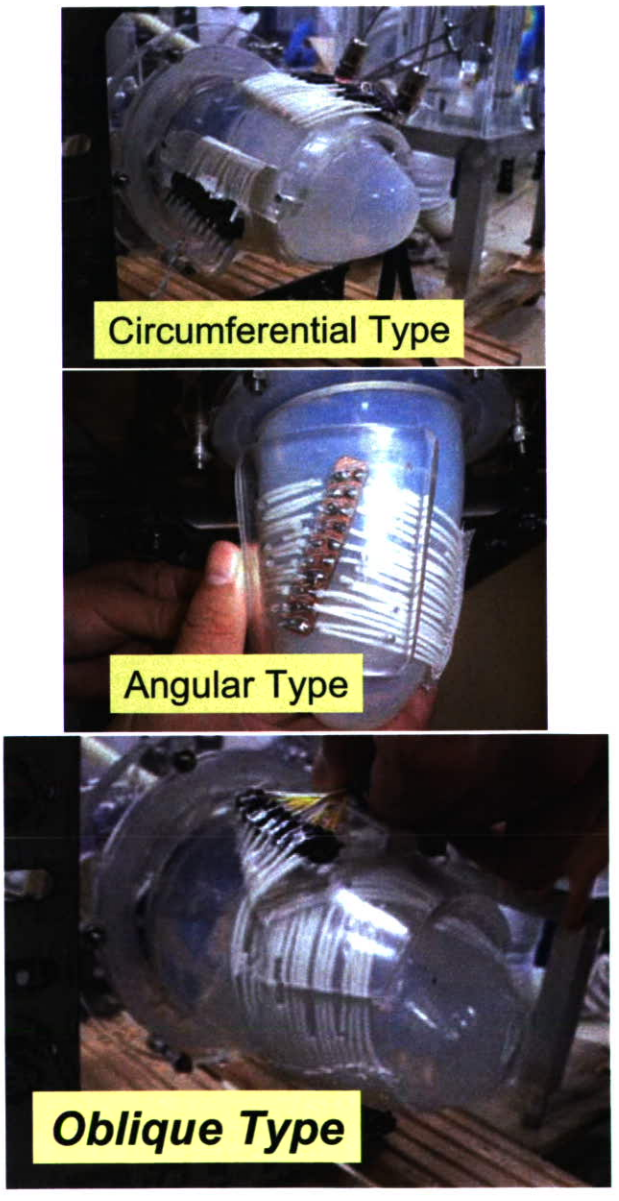

Fig.4: Three different types of the myocardial assist device developed: the oblique type at the bottom could represent the natural oblique stream of myocardial tissue around the left ventricle.

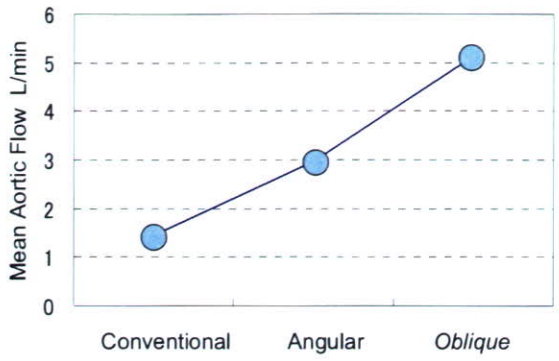

Fig. 5: Changes in mean aortic flow (ventricular model output) obtained from the mechanical circulatory system by using three different configuration types of myocardial assist device.

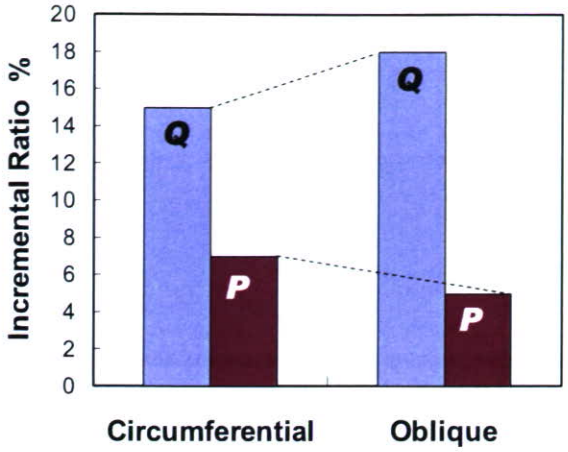

Fig. 6: Changes in the incremental ratio of the hemodynamic data with assistance; P: aortic systolic pressure, Q: aortic flow

the surgical procedure might be simpler compared with other ventricular assist systems. And also the complications, such as thrombosis or hemolysis, would not be caused by this myocardial assist device.

The aortic flow rate was increased by 15% and the systolic left ventricular pressure was elevated by 7% under the cardiac output condition of 3L/min by using the conventional circumferential type. And consequently, the incremental ratio of the left ventricular output was elevated to 18% by using the newly-designed oblique type as showin in Figure 6.

However, any other complications which might have been caused by the operation, such as the disorder of natural autonomic nervous system, were not confirmed in goats yet. As the remarkable increase of the hemodynamic data could be obtained, it was suggested that the effective assistance might be achieved by using this artificial myocardium.

IV. Conclusion

The improvement of an artificial myocardium using the sophisticated covalent shape memory alloy fibres was achieved, which was capable of being installed into the thoracic cavity as the epicardial actuator. As the load of this myocardial system, which was generated by the natural cardiac function, could be estimated by measuring the electrical resistance of the shape-memory alloy fiber, the mechanical myocardial assistance might be effective for heart failure conditions according to the cardiovascular physiological demand.

As our system could assist natural ventricular functions with physiological demand, it might be applied in patients with exertional heart stroke, as well as the cardiac massage at lifesaving emergency for the recovery from ventricular fibrillation.

Acknowledgment

The authors would like to extend their appreciation to Mr. K. Kikuchi and Mr. T. Kumagai for their cooperation in the experiments.

References

[1] Hosenpud JD, et al., "The registry of the international so-ciety for heart and lung transplantation: fifteenth offi-cial report–1998," *J Heart Lung Transplant*, 17, pp. 656–68, 1998

[2] Shimizu T, et al., "Fabrication of pulsatile cardiac tissue grafts using a novel 3-dimensional cell sheet manipulation technique and temperature-responsive cell culture surfaces," *Circ Res*, 90(3), e40, Feb 2002.

[3] Shiraishi Y, et al., "Development of an artificial myocardium using a covalent shape-memory alloy fibre and its cardiovascular diagnostic response" Proc of 2005 IEEE 27th EMBS 0-7803-8740-6/05, 2005

[4] Yambe T, et al., "Addition of rhythm to non-pulsatile circulation," *Biomed Pharmacother*, 58 Suppl 1:S145-9, 2004.

[5] Yambe T, et al., "Artificial myocardium with an artificial baroreflex system using nano technology," *Biomed Pharmacother*, 57 Suppl 1:122s-125s, 2004.

[6] Wang Q, et al., "An artificial myocardium assist system: electrohydraulic ventricular actuation improves myocardial tissue perfusion in goats," *Artif Organs*, 28(9), pp. 853-857, 2004..

[7] Anstadt GL, et al., "A new instrument for prolonged mechanical massage," *Circulation*, 31(Suppl. II), p.43, 1965.

[8] Anstadt M, et al., "Direct mechanical ventricular actruator," *Resuscitation*, 21, pp. 7-23, 1991.

[9] Kawaguchi O, et al., "Dynamic cardiac compression improves contractile efficiency of the heart," *J Thorac Cardiovasc Surg*, 113, pp. 923-31, 1997.

[10] Buehler WJ, Gilfrich J, Wiley KC, "Effect of low-temperature phase changes on the mechanical properties of alloys near composition TiNi," *J Appl Phys*, 34, p.1465, 1963.

[11] Homma D, Miwa Y, Iguchi N, et al., "Shape memory effect in Ti-Ni alloy during rapid heating," *Proc of 25th Japan Congress on Materials Research*, May 1982.

[12] Sawyer PN, et al., "Further study of NITINOL wire as contrctile artificial muscle for an artificial heart," *Carrdiovasc Diseases Bull. Texas Heart Inst* 3, p. 65, 1976.

[13] Torrent-Guasp F, et al., "Structure and function of the heart. Revista Espanola de Cardiologia; 51(2):91-102,1998

[14] Uematsu M, et al., "An innovative approach to evaluate a cardiac functions based on surface measurement", Proc of IEEE 27th EMBS, 0-7803-8740-6/05, 2005.

Proceedings of the 29th Annual International
Conference of the IEEE EMBS
Cité Internationale, Lyon, France
August 23-26, 2007.

Ultrasound Speed and Impedance Microscopy for *in vivo* Imaging

Yoshifumi Saijo, Naohiro Hozumi, Kazuto Kobayashi, Nagaya Okada, Toshimichi Ishiguro, Yoshihiro Hagiwara, Esmeraldo dos Santos Filho and Tomoyuki Yambe

Abstract— **Ultrasound speed and impedance microscopy was developed in order to develop *in vivo* imaging system. The sound speed mode realized non-contact high resolution imaging of cultured cells. This mode can be applied for assessment of biomechanics of the cells and thinly sliced tissues. The impedance mode visualized fine structures of the surface of the rat's brain. This mode can be applied for intra-operative pathological examination because it does not require slicing or staining.**

I. Introduction

Acoustic microscopy for medicine and biology has been developed for more than twenty years at Tohoku University [1-10]. Application of acoustic microscopy in medicine and biology has three major features and objectives. First, it is useful for intra-operative pathological examination because staining is not required. Second, it provides basic acoustic properties to assess the origin of lower frequency ultrasonic images. Third, it provides information on biomechanics at a microscopic level.

In the present study, ultrasonic microscopy that has two measurement modes, sound speed mode for visualization of single-layered cells and impedance mode for visualization of tissue surface, is proposed.

II. Methods

A. Instruments

Fig. 1 shows the block diagram of the ultrasonic speed and impedance microscopy. An electric impulse was generated by a high speed switching semiconductor. The start of the pulse was within 400 ps, the pulse width was 2 ns, and the pulse voltage was 40 V. The frequency of the impulse covered up to 380 MHz. The electric pulse was used to excite a transducer that had a central frequency of 300 MHz and a sapphire rod as an acoustic lens. The ultrasound spectrum of the reflected ultrasound was broad enough to cover 220-380 MHz (-6dB). The reflections from the tissue was received by the transducer and were introduced into a Windows-based PC (Pentium D, 3.0 GHz, 2GB RAM, 250GB HDD) via a digital oscilloscope (Tektronix TDS7154B, Beaverton, USA). The frequency range was 1 GHz, and the sampling rate was 20 GS/s. Four pulse echo sequences were averaged for each scan point in order to increase the signal-to-noise-ratio.

The transducer was mounted on an X-Y stage with a microcomputer board that was driven by the PC through RS232C. The Both X-scan and Y-scan were driven by linear servo motors.

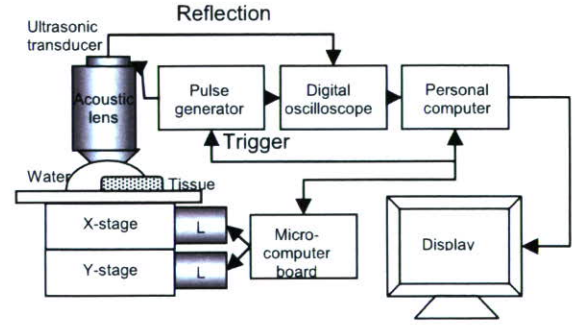

Fig. 1. Block diagram of ultrasonic speed and impedance microscopy

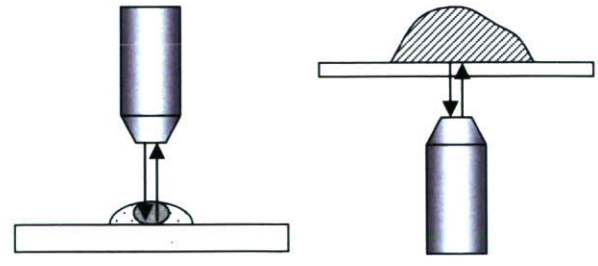

Fig. 2. Schematic illustration of two measurement modes in ultrasonic speed and impedance microscopy. Left: sound speed mode, right: impedance mode

The ultrasonic speed and impedance microscopy has two different modes for observation. Fig. 2 shows the schematic illustration of the relation between the beam propagation and

Manuscript was accepted on June 6, 2007. This work was supported in part by Research Grants from the Ministry of Health, Labor and Welfare for the Research on Advanced Medical Technology (H17-Nano-001) and Grants from New Energy and Industrial Technology Development organization (06001905-0).

Yoshifumi Saijo is with the Institute of Development, Aging and Cancer, Tohoku University, Sendai, 980-8575 Japan (phone: +81-22-717-8514; fax: +81-22-717-8518; e-mail: saijo@ idac.tohoku.ac.jp).

Naohiro Hozumi is with Aichi Institute of Technology, Toyota, Japan. Kazuto Kobayashi, Nagaya Okada and Toshimichi Ishiguro are with Honda Electronics Co. Ltd., Toyohashi, Japan. Yoshihiro Hagiwara is with the Department of Orthopedic Surgery, Graduate School of Medical Science, Tohoku University, Sendai, Japan. Esmeraldo dos Santos Filho and Tomoyuki Yambe are with the Institute of Development, Aging and Cancer, Tohoku University, Sendai, Japan.

1-4244-0788-5/07/$20.00 ©2007 IEEE

the tissue. The left figure shows the sound speed mode for precise imaging (classical acoustic microscopy). The ultrasound propagates through the thinly sliced specimen or cultured cells and reflects at the interface between the specimen and substrate. The right figure shows the impedance mode (acoustic impedance imaging). The ultrasound propagates through the thin plastic plate and is reflected at the interface between plastic and tissue.

B. Tissue Preparation

Sound speed mode is mainly used for visualization of thinly sliced tissues or monolayered cultured cells. In the present study, cultured fibroblast cells were observed by the transmission mode of the ultrasonic imaging system. Fibroblasts were cultured on 35 mm diameter dishes with the Dulbecco's modified Eagle's medium and 10% heat-incubated bovine serum. The incubator was maintained at 37 °C and filled with 95% air and 5% CO_2. After 4days of culture, cells were found to be in the confluent state by inverted microscopy.

Impedance mode can be applied for visualization of tissue surface without thinly slicing the biological tissue. Rats were dissected and the whole brain was removed. A sagittal section of the brain was prepared by a rotor slicer. The specimen was rinsed and preserved in phosphate buffered saline. For optical observation, some adjacent slices were subjected to immuno-histochemical staining against calbindin D-28k.

C. Signal Processing

1) Sound speed Mode

Reflected waveforms are shown in Fig. 3. The waveform at the tissue area is shown in red line and that from substrate is shown in black line. Both signals were captured on the same line in x-scanning.

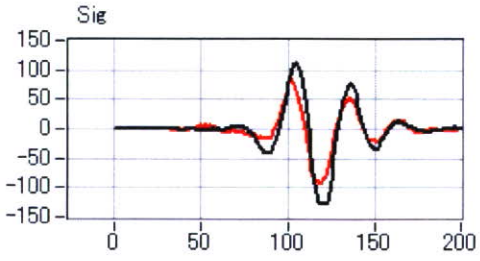

Fig. 3. The waveform at the tissue area (red line) and substrate (black line).

The power spectrum of the reflection at the tissue area is shown in Fig. 4. The spectrum covers the frequency up to 500 MHz. The reflection from the tissue area contains two components. One is from the tissue surface and another from the interface between the tissue and substrate. Frequency domain analysis of the reflection enables the separation of two components [11].

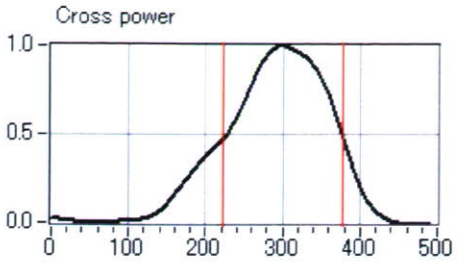

Fig. 4. The power spectrum of the reflection at the tissue area.

Fig. 5 shows the response to a singlet. The left black wave is the reflection from the tissue surface and the right red wave is the reflection from the substrate. These signal processing enables the calculation of tissue thickness and speed of sound.

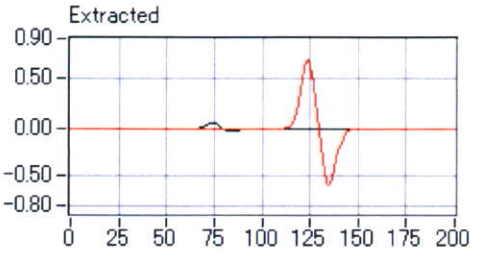

Fig. 5. Response to a singlet. Reflection from he tissue surface (black) and from the substrate (red).

2) Impedance Mode [12]

The target signal is compared with the reference signal and interpreted into acoustic impedance as

$$Z_{target} = \frac{1-\frac{S_{target}}{S_0}}{1+\frac{S_{target}}{S_0}} Z_{sub} = \frac{1-\frac{S_{target}}{S_{ref}} \cdot \frac{Z_{sub}-Z_{ref}}{Z_{sub}+Z_{ref}}}{1+\frac{S_{target}}{S_{ref}} \cdot \frac{Z_{sub}-Z_{ref}}{Z_{sub}+Z_{ref}}} Z_{sub} \cdots (1)$$

where S_0 is the transmitted signal, S_{target} and S_{ref} are reflections from the target and reference, Z_{target}, Z_{ref} and Z_{sub} are the acoustic impedances of the target, reference and substrate, respectively[3].

In case of using water as the reference, its acoustic impedance was assumed to be 1.5 x 10^6 Ns/m^3. On the other hand, in case of using silicon rubber, the acoustic impedance of itself was calibrated, by using water as the standard reference material. In this report, 0.965 x 10^6 Ns/m^3 was used. The acoustic impedance of the substrate was calculated to be 3.22 x 10^6 Ns/m^3, considering its sound speed and density.

III. Results

Fig. 6 and Fig. 7 show the images obtained with the ultrasonic speed and impedance microscopy. Fig. 6 shows the cultured fibroblasts by sound speed mode. The high intensity area at the central part of the cell corresponds to the nucleus (N) and the high intensity area at the peripheral zone corresponds to the cytoskeleton (C) mainly consisted of actin

filaments.

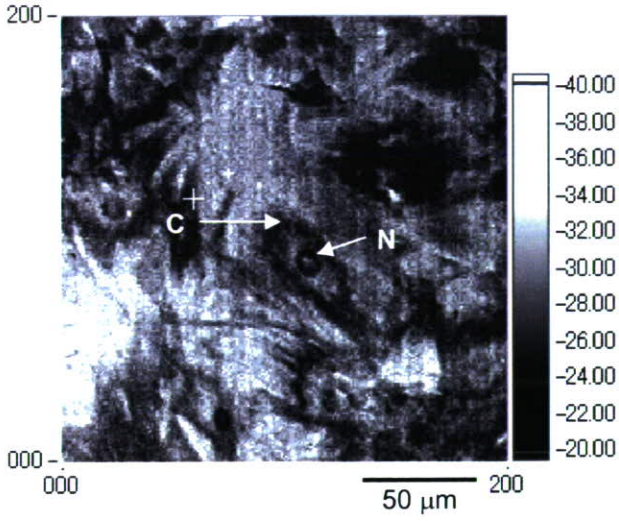

Fig. 6. Fibroblast image obtained with sound speed mode.

Fig. 7 shows the brain of rat by impedance mode. Four layers are visible; molecular layer (ML), Purkinje layer (PL), internal granular layer (IGL) and white matter (WM) in mature cerebellum. Parallel fibers in ML are axon of granule cells and play an important role in cerebella neural connection. Migrating granule cells elongate them horizontally and form a lot of excitatory synapses to dendrite of Purkinje cells. These are major neuronal circuits of cerebellum so that parallel fibers are expected to construct rich ML with development.

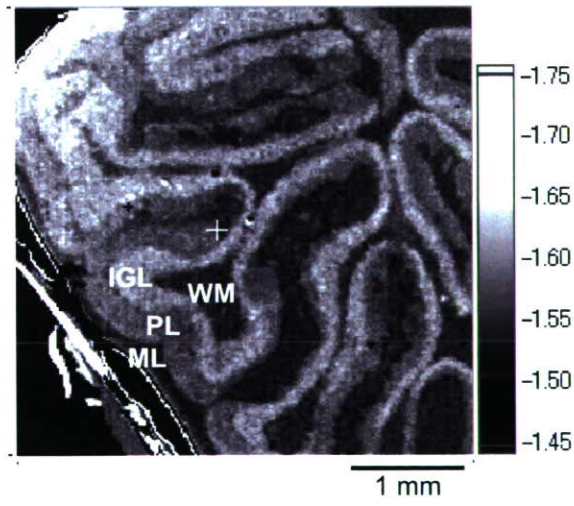

Fig. 7. Rat brain image obtained with impedance mode.

IV. Discussions

Histology has remained the acknowledged "gold standard" for cancer diagnosis or rejection diagnosis in heart transplantation because no other method has been shown to fulfill this requirement consistently. However, biopsy has some limitations and bears a small risk for the patient. For the better quality of life of patients and reducing medical cost for follow up, the method that rapidly, non-invasively and reliably identifies malignant cells or rejection-induced myocardial changes is desired. The final goal of the present study is to realize ultrasonic *in vivo* nano-imaging system that can visualize nano-scale structure of the living organ during the surgical procedure.

In order to achieve the goal, ultrasonic speed and impedance microscopy with two measurement modes was developed. Sound speed mode has been also used in the conventional scanning acoustic microscopy. An ultrasonic transducer with the frequency range up to 380 MHz was fabricated and scanning width was 100 nm to realize 800 nm resolution imaging. This imaging mode however requires the thin objects such as thinly sliced tissue or single layered cultured cells. Impedance mode was developed to break these limitations of conventional acoustic microscopy. The thin plastic plate was set upon the transducer and the image if the surface of the tissue is visualized by contacting the tissue. This mode can be applied for intra-operative histological examination at microscopic level in case the pre-operative examination cannot be performed, for example, brain surgery for treatment of epilepsy or left ventricular reduction surgery. This mechanism may also be applied for endoscopic ultrasound by miniaturizing the parts for mechanical scan.

V. Conclusions

Ultrasonic speed and impedance microscopy with two measurement modes was developed in order to develop *in vivo* imaging. The system realized high precision imaging of cells by sound speed mode and direct visualization of tissue by impedance mode. The combination of the two measurement mode would enable to measure in vivo density and other parameters useful in studies of biomechanics.

Acknowledgment

Yoshifumi Saijo thanks Dr. Sachiko Yoshida with the Toyohashi University of Technology for the experiments on rat brain.

References

[1] M. Tanaka, H. Okawai, N. Chubachi, J. Kushibiki, T. Sannomiya, "Propagation properties of ultrasound in acoustic microscopy through a double-layered specimen consisting of thin biological tissue and its holder," *Jpn J Appl Phy* 23 (1984), pp. 197-199.

[2] Y. Saijo, M. Tanaka, H. Okawai, F. Dunn, "The ultrasonic properties of gastric cancer tissues obtained with a scanning acoustic microscope system," *Ultrasound Med Biol* 17 (1991), pp. 709-714.

[3] H. Sasaki, M. Tanaka, Y. Saijo, H. Okawai, Y. Terasawa, S. Nitta, K. Suzuki, "Ultrasonic tissue characterization of renal cell carcinoma tissue," *Nephron* 74 (1996), pp. 125-130.

[4] Y. Saijo, M. Tanaka, H. Okawai, H. Sasaki, S. Nitta, F. Dunn, "Ultrasonic tissue characterization of infarcted myocardium by scanning acoustic microscopy," *Ultrasound Med Biol* 23 (1997), pp. 77-85.

[5] Y. Saijo, H. Sasaki, H. Okawai, S. Nitta, M. Tanaka, "Acoustic properties of atherosclerosis of human aorta obtained with

high-frequency ultrasound," *Ultrasound Med Biol* 24 (1998), pp. 1061-1064.

[6] Y. Saijo, H. Sasaki, M. Sato, S. Nitta, M. Tanaka, "Visualization of human umbilical vein endothelial cells by acoustic microscopy," *Ultrasonics* 38 (2000), pp. 396-399.

[7] Y. Saijo, T. Ohashi, H. Sasaki, M. Sato, C.S. Jorgensen, S. Nitta, "Application of scanning acoustic microscopy for assessing stress distribution in atherosclerotic plaque," *Ann Biomed Eng* 29 (2001), pp. 1048-53.

[8] H. Sasaki, Y. Saijo, M. Tanaka, S. Nitta, "Influence of tissue preparation on the acoustic properties of tissue sections at high frequencies," *Ultrasound Med Biol* 29 (2003), pp. 1367-72.

[9] Y. Saijo, T. Miyakawa, H. Sasaki, M. Tanaka, S. Nitta, "Acoustic properties of aortic aneurysm obtained with scanning acoustic microscopy," *Ultrasonics* 42 (2004), pp. 695-698.

[10] H. Sano, Y. Saijo, S. Kokubun, "Material properties of the supraspinatus tendon at its insertion – A measurement with the scanning acoustic microscopy," *J Musculoskeletal Res.* 8 (2004), pp. 29-34.

[11] N. Hozumi, R. Yamashita, C.K. Lee, M. Nagao, K. Kobayashi, Y. Saijo, M. Tanaka, N. Tanaka, S. Ohtsuki, "Time–frequency analysis for pulse driven ultrasonic microscopy for biological tissue characterization," *Ultrasonics* 42 (2004), pp. 717-722.

[12] N. Hozumi, A. Kimura, S. Terauchi, M. Nagao, S. Yoshida, K. Kobayashi & Y. Saijo, "Acoustic impedance micro-imaging for biological tissue using a focused acoustic pulse with a frequency Range up to 100 MHz," *Proc 2005 IEEE Int Ultrason Symp* (2005), pp. 170-173.

J Artif Organs (2007) 10:223–227
DOI 10.1007/s10047-007-0395-y

ORIGINAL ARTICLE

Hongjian Liu, PhD · Yun Luo, PhD · Masaru Higa, PhD
Xiumin Zhang, PhD · Yoshifumi Saijo, MD, PhD
Yasuyuki Shiraishi, PhD · Kazumitsu Sekine, PhD
Tomoyuki Yambe, MD, PhD

Biochemical evaluation of an artificial anal sphincter made from shape memory alloys

Abstract Severe anal incontinence is a socially incapacitating disorder and a major unresolved clinical problem that has a considerable negative impact on quality of life. In this study, we developed a new artificial anal sphincter using shape memory alloys (SMAs) in order to improve the quality of life of such patients and evaluated the influence of this sphincter on blood serum chemistry in animal experiments. The artificial anal sphincter was driven by two Ti-Ni SMA actuators sandwiching the intestine and was implanted in three female goats. Blood was collected from the jugular vein on days 1 and 4; at weeks 1 and 2; and at months 1, 2, and 3, postoperatively. Biochemical parameters including total protein, albumin, total bilirubin, aspartate aminotransferase, blood urea nitrogen, creatinine, and C-reactive protein were examined. The time courses of total bilirubin and aspartate amino transferase of the three goats were within the baseline levels after 1 week of implantation and remained normal, demonstrating no liver function complications. The blood urea nitrogen and creatinine levels remained within the normal range, indicating no renal function complications. The total protein and albumin fluctuated within the normal range throughout the duration of this study. In these goats, it was also found that the level of C-reactive protein did not increase and that there was no stricture of the intestine where the artificial sphincter was attached. Our findings indicate that the artificial sphincter SMA demonstrated no adverse influence on blood serum chemistry and exhibited an effective system performance.

Key words Shape memory alloys · Artificial anal sphincter · Biochemical evaluations · Implantation · Goat

Introduction

Severe anal incontinence (incontinence for gas, feces, or both) is a socially incapacitating disorder and a major unresolved clinical problem that has a considerable negative impact on quality of life. This condition is caused by colostomy or ileostomy, neuromuscular disorders, congenital anorectal malformation, and obstetric injury.[1] As a treatment for such patients, an artificial anal sphincter (AMS800, American Medical Systems, Minneapolis, MN, USA) was developed and has been implanted in animal models and patients. However, it has been indicated that the artificial sphincter may not withstand prolonged use because of mechanical failure and structures using a liquid drive mechanism.[1,2]

Nickel–titanium (Ni-Ti) shape memory alloys (SMAs) have many unique mechanical and material characteristics combined with good biocompatibility. SMAs are attracting considerable attention as core materials in medical applications because of their high ratio of recovery force to weight and large recoverable strains. SMAs are durable and can endure up to 50000 cycles of heating and cooling.[3,4] We have previously reported the development of artificial anal sphincters using SMAs for treating patients with neuromuscular disorders, severe congenital anomalies, or colostomy.[3,5] The artificial anal sphincter has only one deformable part and therefore has a simple structure with good durability and is expected to reduce the possibility of mechanical failure. In this study, we evaluated the influence of the artificial anal sphincter on blood serum chemistry in animal experiments.

Received: March 6, 2007 / Accepted: July 31, 2007

H. Liu (✉) · Y. Saijo · Y. Shiraishi · K. Sekine · T. Yambe
Department of Medical Engineering and Cardiology, Institute of Development, Aging and Cancer, Tohoku University, 4-1 Seiryo-machi, Aoba-ku, Sendai 980-8575, Japan
Tel. +81-22-717-8517; Fax +81-22-717-8518
e-mail: hongjianliu63@yahoo.co.jp

Y. Luo · M. Higa
Biomedical Engineering Research Organization, Tohoku University, Sendai, Japan

X. Zhang
Department of Medicine and Science in Sports and Exercise, Tohoku University Graduate School of Medicine, Sendai, Japan

Materials and methods

Animals

Three female goats weighing 50–60 kg were used. The animal experiments were performed after approval by the Research Animal Resource Committee of the Institute of Experimental Animals, Tohoku University School of Medicine, Japan.

Artificial anal sphincter device

The artificial sphincter (AS) is driven by two Ti-Ni SMA actuators sandwiching the intestine. The composition of SMA used in this study was Ti51at%Ni on an atomic basis. The actuator consists of two SMA plates (70 × 18.5 × 0.7 mm) jointed by hinges at their ends and foil type heaters attached on the SMA plates. Silicone pillows were placed on the surfaces of the SMA plates to prevent pressure concentration on the intestines, which may cause ischemia. The bilateral ends of two SMA plates of circumferential shape were fixed with latches, and the alimentary tract was placed between the two SMA actuators.

To control the opening and closing of the anal canal, two meander winding 0.2-mm wires were attached on the surface of each SMA plate as heaters. On heating, the reverse R-phase transformation occurred in the SMA plates, accompanied by shape changes from a flat shape to an arc shape. The shape change resulted in a lumen between the two SMA plates, which allowed bowel movement to take place.

The power to heat the SMA plates can be provided percutaneously by a DC/AC external power supply. A transcutaneous energy transmission system (TETS) was used to supply power to the AS. This system consisted of two coils, one outside the body (primary coil) and the other inside the body (secondary coil). A temperature-responsive reed switch (TRS, TDK, TR-55B50, Tokyo, Japan) was used to prevent overheating of the AS. When an electric current of 4 A at 4 V was supplied, the temperature of the SMA plates immediately started to rise, and the two plates bent to form an almond shape at a temperature of 55°C with a maximal gap of 33 mm between the plates. When the electric current was removed, the SMA plates recovered their initial shapes on natural cooling, resulting in closure of the intestines once again (Fig. 1).

Implantation of the artificial anal sphincter

The animals were placed on a surgical table in the lateral position under general anesthesia and were prepped and draped in sterile fashion. Anesthesia applied by halothane inhalation via a respirator was maintained throughout the procedure.

The creation of end-colostomy on the abdomen through the oblique muscles and the implantation of the artificial SMA anal sphincter were performed. The artificial anal sphincter and overheating protector were implanted between the peritoneum and abdominal wall. The colostomy was reached via an extraperitoneal approach and a space around it was created. The artificial anal sphincter was attached to the intestine with latches. The secondary coil

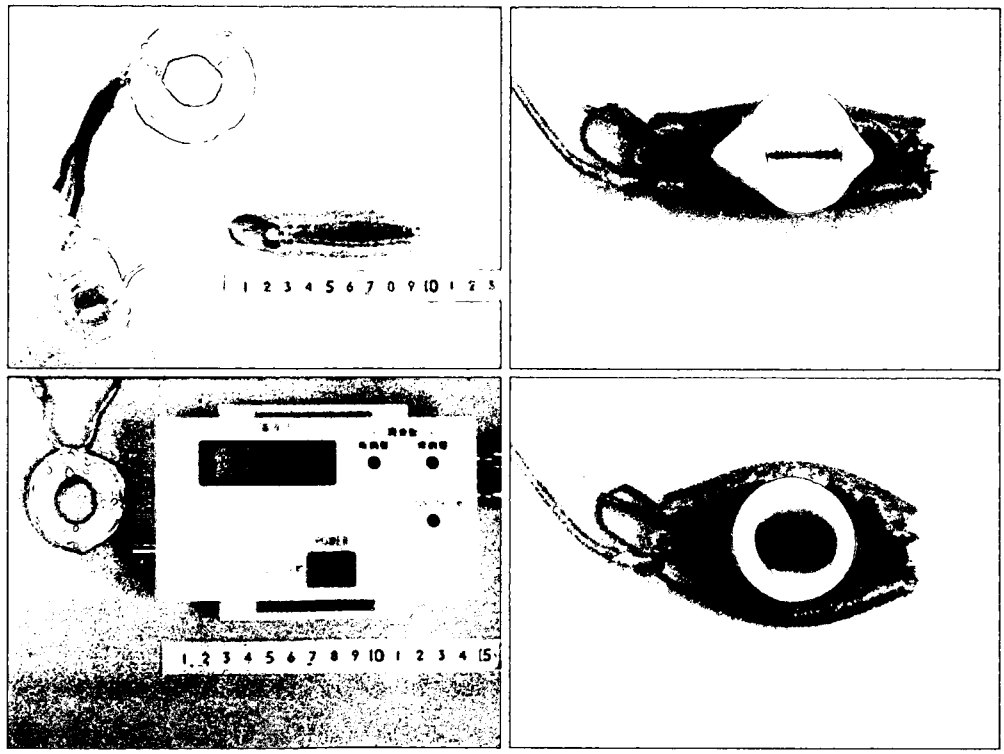

Fig. 1. Implantable components and transcutaneous energy transmission system of a shape memory alloy (SMA) artificial sphincter (AS). *Top left*, implanted components; *bottom left*, extracorporeal components; *top right*, closed state; *bottom right*, open state

was placed in the subcutaneous space near the colostomy, and the primary coil was attached to the skin, aligned with the secondary coil (Fig. 2). The lines to supply electric current to the device were led outside through a subcutaneous tunnel. An antibiotic was administrated intravenously for 3 days after surgery, and feeding was started on the day after the surgery. The bowels of the goats were moved 10 times a day by supplying electricity to the primary coil for 10 min.

Test of biocompatibility

Blood was collected from the jugular vein on days 1 and 4; at weeks 1 and 2; and at months 1, 2, and 3, postoperatively. The blood was centrifuged at 3000 rpm for 10 min to obtain the blood components from the supernatant for hematological examinations. Biochemical parameters including total protein, albumin, total bilirubin, aspartate aminotransferase (AST), blood urea nitrogen, creatinine, and C-reactive protein (CRP) were examined. The animals were killed 3 months after surgery under anesthesia, and tissue samples were collected from the intestine, liver, and kidneys and were preserved in 10% formalin.

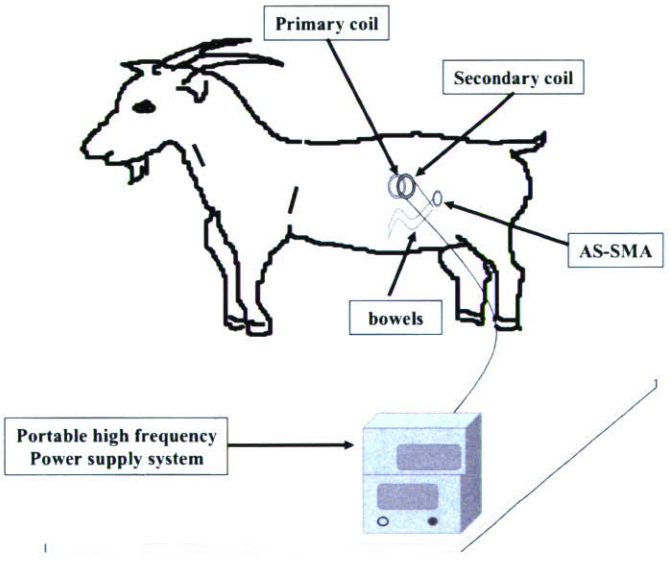

Fig. 2. Chronic animal experiment of a goat implanted with the AS-SMA

Results

In this study, the duration of the three long-term implants of the artificial anal sphincter (i.e., more than 1 week) ranged from 30 to 90 days. The data at 3 months from two of the goats could be recorded; however, the third goat was eliminated from the trial one month after the procedure due to failure of the electrodes.

The device was operated 300 times in 1 month; bowel movements were observed and the stools appeared the same as those seen before implantation. The stoma was always continent in the resting position of the AS, and the goats had a good appetite with no abdominal distension. Macroscopically, the stoma had a ruddy complexion and exhibited elasticity; there was no stricture of the intestine where the AS was attached.

Throughout the study period, the major biochemistry parameters were almost always within the normal ranges. The time courses of total bilirubin and AST of the three goats were within the baseline levels after 1 week of implantation and remained normal, indicating that there were no liver function complications (Fig. 3). The blood urea nitrogen and creatinine levels of the three goats remained within the normal range, demonstrating no renal function complications (Fig. 4). The total protein and albumin levels fluctuated within the normal ranges throughout the study period (Fig. 5), and in these goats, we also found that the level of CRP had not increased during the study.

The developed SMA artificial sphincter (AS-SMA) was implanted in animal models for chronic experiments of up to 3 months duration and exhibited good performance in maintaining fecal continence.

Discussion

The normal biochemistry results observed throughout this study bodes well for the future clinical use of the AS-SMA. Different hematological parameters were evaluated for in vivo assessment of biochemistry. The effects of the AS-SMA on renal and liver functions were evaluated by changes in total creatinine, blood urea nitrogen, bilirubin, and AST. In one goat, abnormal AST and bilirubin levels were evident on postoperative day 4, but these had returned to the normal range by postoperative day 7. The use of halothane anes-

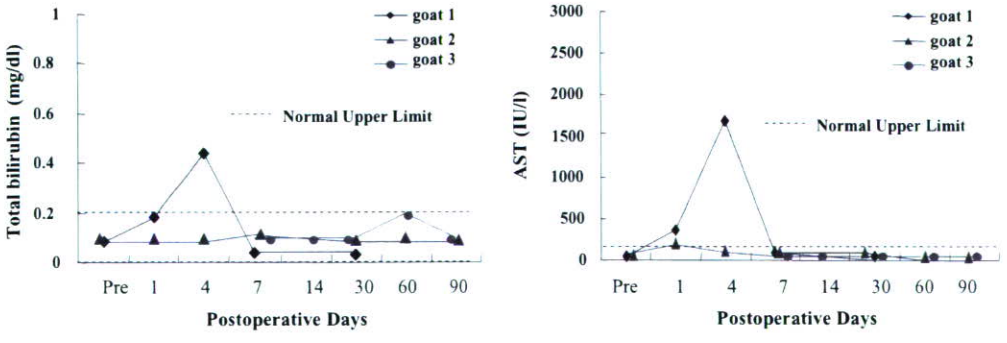

Fig. 3. Total bilirubin and aspartate aminotransferase (*AST*) levels as markers of liver function

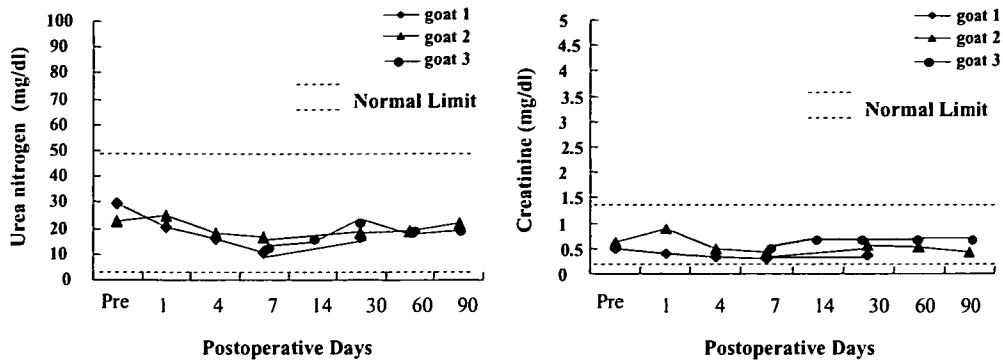

Fig. 4. Urea nitrogen and creatinine levels as markers of renal function

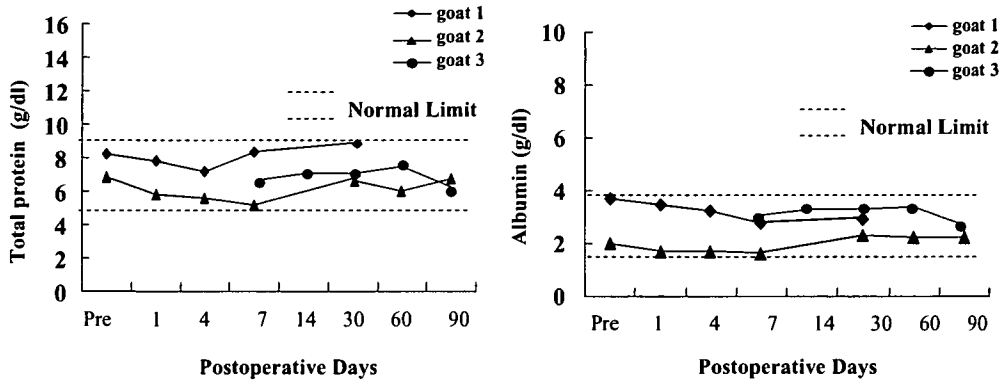

Fig. 5. Total protein and albumin levels as markers of nourishment state

thesia can induce an elevation of serum activities of liver enzymes, often around 2 to 7 days after anesthesia, and the leakage of enzyme into the serum may have come from muscle damage at the time of surgery.

Chronic in vivo studies of the AS-SMA in three goats demonstrated little influence on blood serum chemistry and showed the reliability and effective performance of the system. There were no incidences of bleeding, systemic organ dysfunction, or mechanical failure in any of the goats. Of the three long-term implanted goats, one goat was terminated after 30 days because of electrode-related issues, and two goats were terminated after 90 days. The failure of the electrodes was consistent with moisture permeation; device-related difficulties were limited to just two cable-related issues.[6-12]

Use of this AS-SMA will minimize the surgical invasiveness and compression of the surrounding tissues such as the skin and gastrointestinal system, resulting in a rapid recovery from the surgery and reduced risks of pocket bleeding, wound infection, and malnutrition. Ni-Ti alloys have been reported to exhibit good biocompatibility due to their high corrosion resistance and Ni-Ti alloys have gained popularity in the biomedical field because of their appealing mechanical properties.[11,13-15] The SMA was covered with a silicone pillow and exhibited conformity with the living body in the contact point with the anal canal. The soft silicone pillow covering material reduces the pressure concentration on the contacting area of the intestines and allows good circulation.

In this study, the small loss of power by the TETS resulted in sufficient capability for energy transmission. During the experiment, the AS opened each time energy was transmitted; however, if the efficiency were improved, less AC power would be required. The AS was kept open for 10 min, although the surface temperature was lower than 43°C because the allowable body temperature was around 42°C. The overheating protector was able to prevent burns around the AS and extended the duration of AS opening.[1,4,5]

The AS was opened for a long enough period (10 min) to allow controlled fecal continence. Fecal movements were regularly observed when the artificial anal sphincter was activated, and the evacuated feces were confirmed as being normal.

These biochemistry studies support the concept and design of this implantable artificial anal sphincter. In conclusion, this artificial anal sphincter demonstrated no adverse influence on blood serum chemistry and exhibited an effective system performance.

Acknowledgments This research was supported by the Industrial Technology Research Grant Program in 2000 (00A45027) from the New Energy and Industrial Technology Development Organization (NEDO) of Japan.

References

1. Nishi K, Kamiyama T, Wada M, Amae S, Ishii T, Takagi T, Luo Y, Okuyama T, Yambe T, Hayashi Y, Ohi R. Development of an implantable artificial anal sphincter using a shape memory alloy. J Pediatr Surg 2004;39:69-72
2. Hajivassiliou CA, Carter KB, Finlay IG. Biomechanical evaluation of an artificial anal sphincter prosthesis. J Med Eng Technol 1997;21:89-95

3. Amae S, Wada M, Luo Y, Nakamura H, Yoshida S, Kamiyama T, Yambe T, Takagi T, Nitta S, Ohi R. Development of an implantable artificial anal sphincter by the use of a shape memory alloy. ASAIO J 2001;47:346–350
4. Luo Y, Higa M, Amae S, Takagi T, Yambe T, Okuyama T, Tanaka H, Kakubari Y, Matsuki H. Preclinical development of SMA artificial anal sphincters. Minim Invasive Ther Allied Technol 2006; 15:241–245
5. Luo Y, Takagi T, Okuyama T, Amae S, Wada M, Nishi K, Kamiyama T, Yambe T, Matsuki H. Functional evaluation of an artificial anal sphincter using shape memory alloys. ASAIO J 2004;50: 338–343
6. Jain A, Mohanka R, Orloff M, Abt P, Kashyap R, Cullen J, Lansing K, Bozorgzadeh A. University of Wisconsin versus histidine-tryptophan-ketoglutarate for tissue preservation in live-donor liver transplantation. Exp Clin Transplant 2006;4:451–457
7. Mussivand T, Harasaki H, Litwak K, Slaughter MS, Gray LA Jr, Dowling TR, Mueller R, Masters RG, Hendry PJ, Beck-Da-silva L, Davies R, Haddad H, Mesana TG, Keon WJ. In vivo evaluation of the biocompatibility of the totally implantable ventricular assist device (HeartSaver VAD). ASAIO J 2003;49:459–462
8. Ortiz H, Armendariz P, DeMiguel M, Ruiz MD, Alos R, Roig JV. Complications and functional outcome following artificial anal sphincter implantation. Br J Surg 2002;89:877–881
9. Petrou SP, Elliott DS. Artificial urethral sphincter for incontinence in adults. Drugs Today (Barc) 2001;37:237–244
10. Schenk S, Weber S, Luangphakdy V, Flick CR, Chen JF, Inoue M, Kopcak MW Jr, Ootaki Y, Doi K, Dessoffy R, Hirschman GB, Vitale NG, Chapman PA Jr, Smith WA, Fukamachi K. In vivo performance and biocompatibility of the MagScrew ventricular assist device. ASAIO J 2003;49:594–598
11. Vaizey CJ, Kamm MA, Gold DM, Bartram CI, Halligan S, Nicholls RJ. Clinical, physiological, and radiological study of a new purpose-designed artificial bowel sphincter. Lancet 1998;352:105–109
12. Yokus B, Cakir DU, Kanay Z, Gulten T, Uysal E. Effects of seasonal and physiological variations on the serum chemistry, vitamins and thyroid hormone concentrations in sheep. J Vet Med A Physiol Pathol Clin Med 2006;53:271–276
13. Es-Souni M, Es-Souni M, Fischer-Brandies H. On the transformation behaviour, mechanical properties and biocompatibility of two NiTi-based shape memory alloys: NiTi42 and NiTi42Cu7. Biomaterials 2001;22:2153–2161
14. Thierry B, Tabrizian M, Trepanier C, Savadogo O, Yahia L. Effect of surface treatment and sterilization processes on the corrosion behavior of NiTi shape memory alloy. J Biomed Mater Res 2000; 51:685–693
15. Wilson SK, Delk JR II. Ectopic placement of AMS 800 urinary control system pressure-regulating balloon. Urology 2005;65: 167–170

B-mode and C-mode Imaging of Regenerated 3D Skin Model with 100 MHz Ultrasound

Yoshifumi Saijo
Department of Medical Engineering and Cardiology
Institute of Development, Aging and Cancer, Tohoku University
Sendai, Japan

Yoshihiro Hagiwara
Department of Orthopedic Surgery
Tohoku University School of Medicine
Sendai, Japan

Kazuto Kobayashi, Nagaya Okada
Honda Electronics Co. Ltd.
Toyohashi, Japan

Akira Tanaka
Faculty of Symbiotic Systems Science
Fukushima University
Fukushima, Japan

Naohiro Hozumi
Department of Electrical Engineering
Aichi Institute of Technology
Toyota, Japan

Kenji Tomihata
Gunze Co. Ltd.
Kyoto, Japan

***Abstract*—Regenerated skin with 3D structure is desired for the treatment of large burn and for the plastic surgery. High frequency ultrasound is suitable for non-destructive testing of the skin model because it provides information on morphology and mechanical properties. An acoustic microscope system capable of imaging B-mode and C-mode was developed for analysis of 3D skin model. C-mode imaging provided quantitative values of attenuation and sound speed. B-mode imaging showed fine structure of the model. Sound speed in C-mode and intensity in B-mode imaging showed higher values at the area of dense fibroblasts. The system can be used as the nondestructive evaluation tool in the process of producing 3D skin model and as the in vivo imaging system after transplantation.**

Keywords-component; 3D skin model; acoustic microscopy; B-mode; C-mode

I. INTRODUCTION

A. Current Status of Regenerated Skin

Three-dimensionally regenerated skin with epidermis, dermis, hair follicle, lipid gland and capillary is desired for the treatment of large burn or for plastic surgery. Not only the structure, should the skin model be flexible as normal skin.

Artificial dermis, Pelnac® (Gunze, Kyoto, Japan) was commercialized in Japan in 1996 [1]. Pelnac consisted of collagen sponge covered with silicon film. As it needed autologous epidermis coverage, repeated operation was required.

Cultured epidermis was approved in Japan on October 3, 2007 for orphan use of severe skin burn. Skin biopsy from the patient is performed to obtain autologous epidermis and keratinocytes are isolated from the tissue. Cells are cultured to form sheet structure and finally the sheeted epidermis is transplanted to the patient. As the epidermis is autologous, risk of rejection is avoided [2]. However, the cultured epidermis is only grown in the skin with dermis. Then it cannot be used in the case of severe burn without dermis.

Cultured dermis has the same structure as artificial dermis. Fibroblasts are cultured in the collagen sponge layer of the artificial dermis. The model was slightly advanced from the artificial dermis but it still needed autologous epidermis coverage.

Apligraf® (Organogenesis Inc., Canton, MA, USA) is bi-layered skin substitute consisting of living cells and structural proteins. The lower dermal layer combines bovine type 1 collagen and human fibroblasts (dermal cells), which produce additional matrix proteins. The upper epidermal layer is formed by promoting human keratinocytes (epidermal cells) first to multiply and then to differentiate to replicate the architecture of the human epidermis [3].

Another cultured 3D skin model, Vitrolife-Skin® (Gunze, Kyoto, Japan) is 3D human skin model used as an alternative for animal skin during irritation test. Keratinocytes are cultured to cover cultured epidermis to form two-layered structure [4].

Fig. 1 shows the schematic illustration of each regenerated skin model.

1051-0117/07/$25.00 ©2007 IEEE

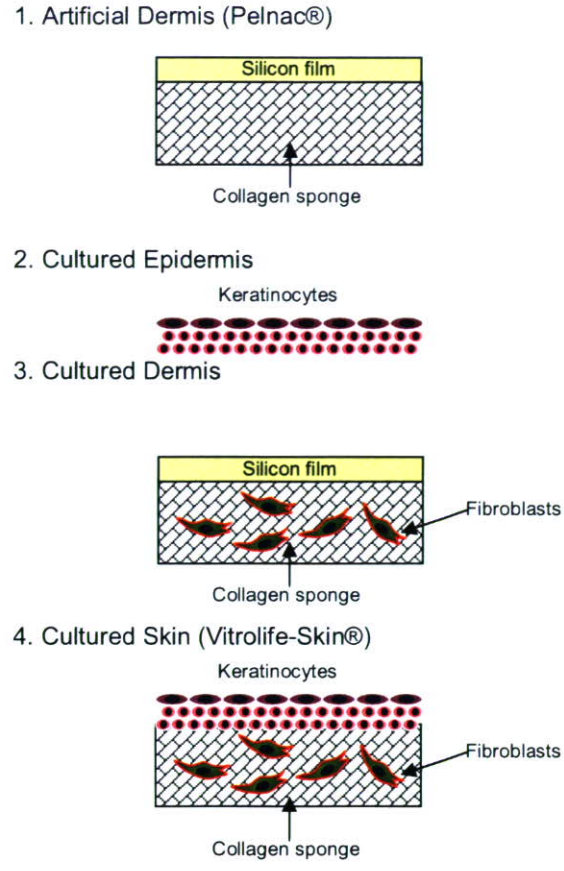

Fig. 1 Schematic illustrations of regenerated skin models

Although these cultured skins have bi-layered structure, they do not contain melanocytes, Langerhans' cells, macrophages, and lymphocytes, or other structures such as blood vessels, hair follicles or sweat glands. As they don't have vasculature, barrier function against bacterial infection is very weak. Their elastic property is different from normal skin because they are lacking elastic fiber.

B. Research and Development of Three-dimensional Complex Organ Structures

The three-dimensional molding methods and noninvasive evaluation techniques are fully employed to realize structures that are morphologically and functionally similar to those of a living body. This will enable the realization of large-size structures, regeneration of organ structures suitable to anatomical morphology, and functional reconstruction by applying various engineering techniques that are difficult to produce with present tissue engineering. At the same time, revascularization in the host site, which is necessary for achieving graft adhesion and self-organization of the three-dimensional complex organ structures, will be realized.

As a part of this research project, 3D skin model with bi-layer structure, elastic fiber and vasculature is aimed and non-invasive repetitive evaluation method is desired. High frequency ultrasound is suitable for non-destructive testing of the skin model because it provides information on morphology and mechanical properties. In the present study, the same plane, which was perpendicular to the skin surface, of the skin model with 3D structure was investigated with both B-mode and C-mode ultrasound imaging using 100 MHz ultrasound.

II. METHOD

A. System Setup

Fig. 2 shows the schematic illustration of the B-mode and C-mode imaging system. An electric impulse was generated by a high speed switching semiconductor. The start of the pulse was within 400 ps, the pulse width was 2 ns, and the pulse voltage was 40 V. The frequency of the impulse covered up to 500 MHz. The electric pulse was used to excite a PVDF transducer with the central frequency of 100 MHz. The ultrasound spectrum of the reflected ultrasound was broad enough to cover 50-160 MHz (-6dB). The reflections from the tissue was received by the transducer and were introduced into a Windows-based PC (Pentium D, 3.0 GHz, 2GB RAM, 250GB HDD) via a high-speed A/D converter (Acqiris DP210, Geneva, Switzerland). The frequency range was 500 MHz, and the sampling rate was 2 GS/s. Eight pulse echo sequences were averaged for each scan point in order to increase the signal-to-noise-ratio. The transducer was mounted on an X-Y stage with a microcomputer board that was driven by the PC through RS232C. The Both X-scan and Y-scan were driven by linear servo motors.

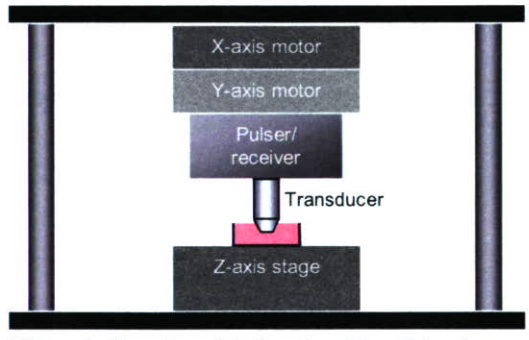

Fig. 2 Schematic illustrations of the B-mode and C-mode imaging system

B. Ultrasonic Transducers

B-mode imaging was obtained with a PVDF transducer with the diameter of 2.4 mm and the focal length of 3.2 mm. C-mode imaging was obtained with a different PVDF transducer with the diameter of 1.8 mm and the focal length of 1.5 mm.

C. Signal Processing

RF signal of each scanning line was converted to B-mode image by a conventional image processing algorithm. The scan area was 2.4 mm x 3.0 mm with 300 x 4000 pixels. Y scan width was available 8 / 16 / 24 / 64 microns step to obtain 3D data set.

The transfer function of the pulsed response at tissue region and glass region was calculated in a frequency domain to calculate the tissue thickness, attenuation and sound speed in C-mode imaging [5-7].

D. Tissue Preparation

Fibroblasts in Vitrolife-Skin were cultured with the Dulbecco's modified Eagle's medium and 10% heat-incubated bovine serum. The incubator was maintained at 37 °C and filled with 95% air and 5% CO_2.

First, B-mode images were obtained by using the saline as the coupling medium. After B-mode evaluation, the sample was frozen and sliced at 5 micron in thickness as to make the same observation plane for C-mode imaging. The neighboring sections of C-mode image were stained with Elastica-Masson staining for optical microscopic observation.

III. RESULTS

Fig. 3 shows (a) optical microscopic and (b) B-mode images of Vitrolife-Skin. Epidermis (E) was observed as a relatively high echoic band by B-mode imaging. Dermis consisted of collagen sponge and fibroblasts had heterogenic echo pattern.

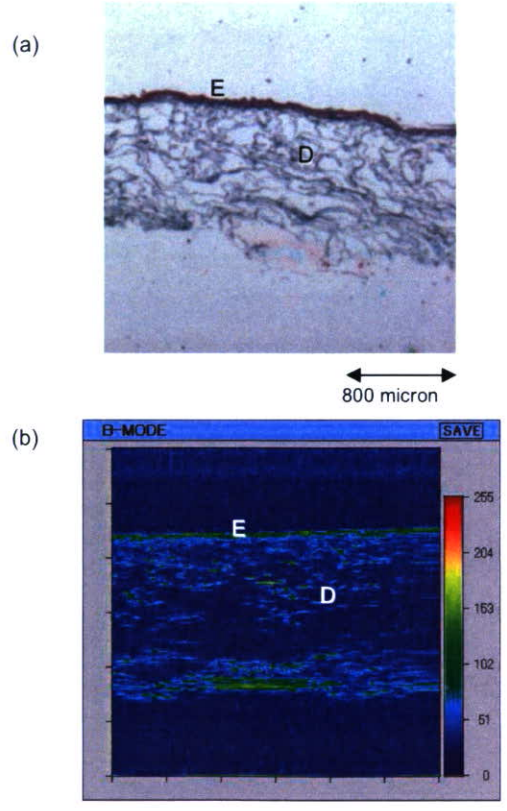

Fig. 3 (a) optical microscopic and (b) B-mode images of Vitrolife-Skin

Fig. 4 shows the (a) optical microscopic and C-mode images ((b): attenuation, (c): sound speed) of Vitrolife-Skin. The sound speed of the epidermis was approximately 1580 m/sand the sound speed of dermis was ranged 1530 to 1560 m/s corresponding to the density of fibroblasts in the dermis.

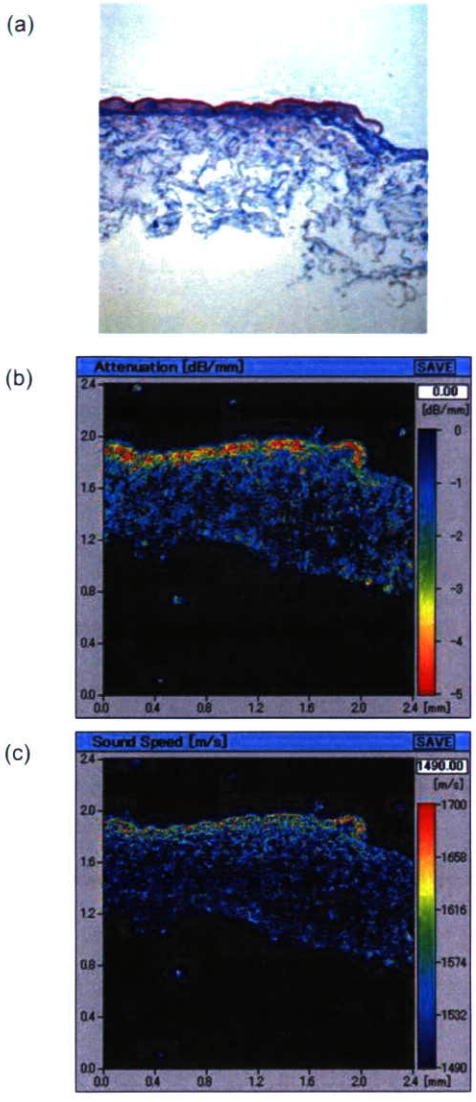

Fig. 4 (a) optical microscopic and C-mode ((b): attenuation, (c): sound speed) images of Vitrolife-Skin

The density of fibroblast (number / 0.2x0.2 mm) and the sound speed of the corresponding region were measured in 12 regions from 6 specimens. Fig. 5 shows the relationship between tow parameters. The result suggests there is a strong relationship between cellularities and sound speed.

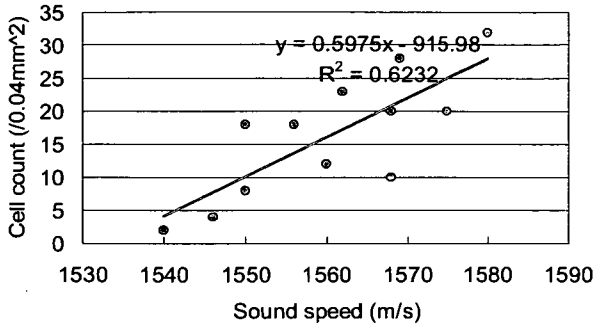

Fig. 5 Relationship between cell count and sound speed

IV. Discussion

Compared with conventional high frequency B-mode imaging modalities, this system is unique because it can be used as C-mode acoustic microscopy. C-mode quantitative values are important for understanding *in vivo* B-mode images. As the spatial resolution of the system is 15 micron, it is enough to visualize epidermis with 50-100 micron thickness. However, dermis consisting of collagen sponge and fibroblasts was hard to visualize in case the cellularties was very sparse.

One of the future directions of this imaging modality is nondestructive testing of the regenerated skin during tissue culture because it can clearly visualize the cellular density in the dermis and because non-invasive, non-contact, non-infectious method is desired for evaluation of skins. It also has a promising future as a medical imaging device. Continuous evaluation during culture and after transplantation can be performed by the same imaging system in the regenerative medicine. It can be used as a diagnostic device in dermatology. As the system clearly shows the thickness of epidermis and mechanical properties represented acoustic parameters, the system is applicable in cosmetic care of skin.

V. Conclusion

Regenerated skin with 3D structure is desired for the treatment of large burn and for the plastic surgery. High frequency ultrasound is suitable for non-destructive testing of the skin model because it provides information on morphology and mechanical properties. An acoustic microscope system capable of imaging B-mode and C-mode was developed for analysis of 3D skin model. C-mode imaging provided quantitative values of attenuation and sound speed. B-mode imaging showed fine structure of the model. Sound speed in C-mode and intensity in B-mode imaging showed higher values at the area of dense fibroblasts. The system can be used as the nondestructive evaluation tool in the process of producing 3D skin model and as the in vivo imaging system after transplantation.

Acknowledgment

This work was supported in part by Research Grants from the Ministry of Health, Labor and Welfare for the Research on Advanced Medical Technology (H17-Nano-001), Grants-in-Aid for Scientific Research (Scientific Research (B) 19300179) from the Japan Society for the Promotion of Science and Grants from New Energy and Industrial Technology Development Organization (06001905-0).

References

[1] S. Suzuki, K. Kawai, F. Ashoori, N. Morimoto, Y. Nishimura, Y. Ikada, "Long-term follow-up study of artificial dermis composed of outer silicone layer and inner collagen sponge," Br. J. Plast. Surg. Vol. 53, pp. 659-66, December 2000.

[2] K. Hata, "Current issues regarding skin substitutes using living cells as industrial materials," J. Artif. Organs, vol. 10, pp. 129-32, 2007.

[3] W.H. Eaglstein, V. Falanga, "Tissue engineering and the development of Apligraf, a human skin equivalent," Clin. Ther. Vol. 19, pp.894-905, September-October 1997.

[4] T. Uchino, H. Tokunaga, H. Onodera, M. Ando, "Effect of squalene monohydroperoxide on cytotoxicity and cytokine release in a three-dimensional human skin model and human epidermal keratinocytes," Biol. Pharm. Bull, vol. 25, pp.605-10, May 2002.

[5] N. Hozumi, R. Yamashita, C.K. Lee, M. Nagao, K. Kobayashi, Y. Saijo, M. Tanaka, N. Tanaka, S. Ohtsuki, "Time-frequency analysis for pulse driven ultrasonic microscopy for biological tissue characterization," Ultrasonics. vol. 42, pp.717-22, April 2004.

[6] Y. Saijo, N. Hozumi, C. Lee, M. Nagao, K. Kobayashi, N. Oakada, N .Tanaka, E.D. Santos Filho, H. Sasaki, M. Tanaka, T. Yambe, "Ultrasonic speed microscopy for imaging of coronary artery," Ultrasonics, vol. 44, pp.e51-5, December 2006.

[7] Y. Saijo, E. Santos Filho, H. Sasaki, T. Yambe, M. Tanaka, N. Hozumi, K. Kobayashi, N. Okada, "Ultrasonic tissue characterization of atherosclerosis by a speed-of-sound microscanning system," IEEE Trans Ultrason. Ferroelectr. Freq. Control, vol. 54, pp.1571-7, August 2007.